

## MIT Open Access Articles

*Computational Design Principles of Two-Center First-Row Transition Metal Oxide Oxygen Evolution Catalysts*

The MIT Faculty has made this article openly available. **Please share** how this access benefits you. Your story matters.

**Citation:** Mavros, Michael G. et al. "Computational Design Principles of Two-Center First-Row Transition Metal Oxide Oxygen Evolution Catalysts." *The Journal of Physical Chemistry C* 121, 29 (July 2017): 15665–15674 © 2017 American Chemical Society

**As Published:** <https://pubs.acs.org/doi/10.1021/acs.jpcc.7b02424>

**Publisher:** American Chemical Society (ACS)

**Persistent URL:** <http://hdl.handle.net/1721.1/115103>

**Version:** Author's final manuscript: final author's manuscript post peer review, without publisher's formatting or copy editing

**Terms of Use:** Article is made available in accordance with the publisher's policy and may be subject to US copyright law. Please refer to the publisher's site for terms of use.



# Computational Design Principles of Two-Center First-Row Transition Metal Oxide Oxygen Evolution Catalysts

Michael G. Mavros,<sup>†</sup> James J. Shepherd,<sup>†</sup> Takashi Tsuchimochi,<sup>†,‡</sup> Alexandra R.  
McIsaac,<sup>†,¶</sup> and Troy Van Voorhis\*,<sup>†</sup>

<sup>†</sup>*Department of Chemistry, Massachusetts Institute of Technology, 77 Massachusetts Ave,  
Cambridge, MA 02139 USA*

<sup>‡</sup>*Graduate School of Science, Technology and Innovation, Kobe University, Kobe 657-8501,  
Japan*

E-mail: tvan@mit.edu

## Abstract

Computational screens for oxygen evolution reaction (OER) catalysts based on Sabatier analysis have seen great success in recent years; however, the concept of using chemical descriptors to form a reaction coordinate has not been put under scrutiny for complex systems. In this paper, we examine critically the use of chemical descriptors as a method for conducting catalytic screens. Applying density functional theory calculations to a two-center metal-oxide model system, we show that the Sabatier analysis is quite successful for predicting activities and capturing the chemical periodic trends expected for the first-row transition metal series, independent of the proposed mechanism. We then extend this analysis to heterodimer metallic systems—metal oxide catalysts with two different catalytically-active metal centers—and find signs that the Sabatier analysis may not hold for these more complex systems. By performing a principle component analysis on the computed redox potentials, we show (1) that a single chemical descriptor inadequately describes heterodimer overpotentials; and (2) mixed-metal

overpotentials cannot be predicted using only pure-metal redox potentials. We believe that the analysis presented in this manuscript shows a need to move beyond the simple chemical descriptor picture when studying more complex mixed metal-oxide OER catalysts.

## Introduction

The oxygen evolution reaction (OER) is a popular proposal to store energy from sources such as the sun in chemical bonds, using the energy to split water and produce hydrogen gas as a fuel,



where  $E^\circ$  is reported with respect to the standard hydrogen electrode (SHE). This reaction can then be reversed, oxidizing hydrogen gas in a fuel cell to produce water and releasing the energy in the process. The oxygen evolution half-reaction occurs efficiently in nature with low activation barriers<sup>1-3</sup>; promoting efficient oxygen evolution artificially is a much larger challenge, due to an ill-understood mechanism and resulting high catalytic overpotentials<sup>4,5</sup>. Catalytic design varies wildly, from small molecule transition metal complexes<sup>6,7</sup> to amorphous cobalt oxides<sup>8</sup> and perovskite materials<sup>9-11</sup>; unfortunately, underlying design principles of these materials are often poorly understood. A deep understanding of the chemistry of these catalysts could be used to screen entire classes of catalysts as a time, predicting which will likely be efficient and which not before ever spending resources to make them.

Computational high throughput screening for materials design is increasingly a reality, since computing power and memory have increased to the point where materials can be treated with sufficient accuracy in reasonable amounts of time. The ultimate goal of a computational screen is to judge the efficacy of a catalyst without knowing the detailed mechanistic workings of a catalytic cycle; after all, for a novel catalyst, these workings are at best unknown, and at worst unknowable. There are two primary approaches to developing a computational screen. One school purports to develop computational screens based on machine learning algorithms, where a computer interpolates the activity of a novel material based on a statistical analysis of the activities of a large

number of existing materials. Machine-learning approaches have been extremely successful in predicting the properties of organic photovoltaic materials<sup>12</sup> as well as metal-oxides<sup>13</sup>, among others, using input from both theoretical calculations and experiment<sup>14</sup>. A second approach is based on understanding the mechanistic details of catalysis and using information about the chemistry to make novel predictions. We adopt the latter approach in this work.

When developing a computational screen of materials based on understanding the chemistry underlying catalysis, a popular approach is to search for and screen based on a *chemical descriptor* for the activity. An effective chemical descriptor is a quantity that can be conveniently calculated for modest cost and that is linearly related to catalytic activity. In ideal cases, a class of catalytic materials can be described using a single descriptor such that as the value of the descriptor is changed, the catalytic activity increases linearly, reaches a cusp, and then decreases linearly, forming what is known as a *volcano plot*<sup>15–18</sup>. On one side of the cusp, one mechanistic step limits the overall rate of catalysis; on the other side of the cusp, a different step limits the overall rate. In this picture, the search for an optimal catalyst is reduced to the search for a material with the optimal value of the chosen chemical descriptor, as these materials are thought to achieve an optimal balance between two competing rate-determining steps.

While useful, framing catalytic screens in terms of chemical descriptors is an oversimplified construct. Realistic catalysts are very complex, and catalytic activities that significantly deviate away from the lines defining a volcano plot is often observed (see, e.g., Reference 19). Even if a descriptor is found to adequately predict activities of a certain class of materials, it almost certainly will not be universal and may not exist at all for entire other classes of catalytic materials. Of particular note is that descriptors which are developed for pure materials may often not hold for combinations of several simple materials, due to complex interactions which do not exist in the pure substance<sup>20</sup>. Nevertheless, due to the simplicity of the descriptor picture, a sizable quantity of literature is devoted to the discovery of such descriptors for OER<sup>17,21–23</sup> and other systems<sup>24–30</sup>. We will review some of that literature now.

Three groups of interrelated descriptors are prevalent in the design of OER. In the first, an orbital/energy level framework, good catalysts are found to have particular 3d states, a good d-

band energy match with  $\text{O}_2$  energy levels, or particular  $e_g$  orbital occupations<sup>9,31</sup>. These descriptors were used to recently find a barium-strontium-cobalt-iron metal oxide with an order of magnitude higher activity than iridium oxides.

A number of authors assert that a universal framework for design can be achieved by considering a second descriptor: surface binding of oxygen, hydroxide, or other intermediates<sup>23</sup>. One of the first examples of this framework is the Sabatier analysis, pioneered in the 1910s<sup>15</sup>, and experimental attempts to use this descriptor to design new catalysts date back to 1955<sup>32</sup>. Recently, Norskov and coworkers have pioneered their use in computational catalytic design through their work on rutile materials<sup>17,33</sup> and metals<sup>16,18,25</sup>. It should come as no surprise that the metal-oxygen bond strength descriptor and the orbital framework descriptor are related, as observed by Vojvodic and Norskov<sup>34</sup>. Sabatier analysis has been used with great success in electrochemical catalysis over the past decade<sup>23,35-39</sup>, in particular guiding the design of certain efficient perovskite catalysts before their experimental realization<sup>9,34,40</sup>.

The final descriptor considers the oxidation of the metal. A 1980 paper by Trasatti suggested metal oxidation would supersede the strength of surface adatom binding as the optimal descriptor<sup>41</sup>. Since descriptors always have linear relationships with the overpotential, it is natural to consider whether the overpotential of alloys can be estimated from a linear combination of their constituents. This approach would prevent the increase of computational complexity when ternary complexes are considered, and has recently found success in the case of the design of a Fe-Co-W alloy for OER<sup>20</sup>.

Once a mechanism is regarded as understood for a single catalyst, chemical descriptors can be derived that allow for screening materials without evaluation of all thermodynamic parameters for an entire mechanism. When two separate mechanisms have separate descriptors, evaluation of the descriptors can be used to discern which mechanism is most likely to be responsible for catalysis. For OER, two popular mechanisms are shown in Figure 1: the acid-base (or water nucleophilic attack) mechanism<sup>7,42,43</sup> and the direct coupling (or radical coupling) mechanism<sup>44-46</sup>. As others have done previously<sup>6,31,46-49</sup>, we will study properties of these mechanistic intermediates to inform OER catalyst design.

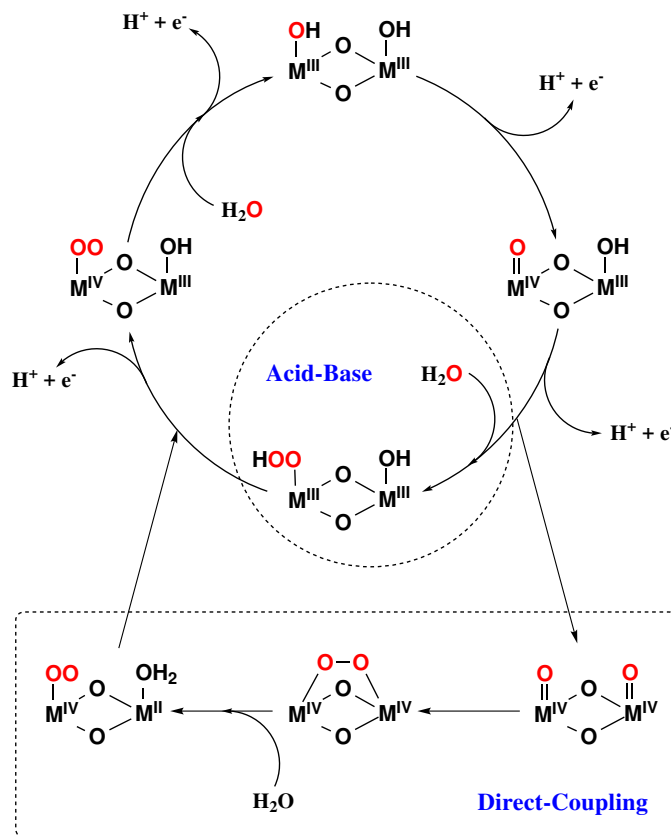


Figure 1: Oxygen evolution can proceed via a variety of mechanisms. In this manuscript, we will focus on the acid-base (also known as water nucleophilic attack) mechanism, where the O-O bond is formed by a nucleophilic attack by water on an oxidized catalyst; and the direct-coupling (or radical coupling) mechanism, where oxygens a doubly-oxidized catalyst snap together to form the O-O bond. For the direct-coupling mechanism, we refer to the steps in order from the top by the following names: (1) Metal(III) first oxidation, (2) Metal(III) second oxidation, (3) O-O bond formation, (4) Water attachment; (5) Metal(II) oxidation, and (6) Oxygen displacement.

In this manuscript, we take a multi-pronged approach to understanding OER catalysis on transition-metal oxides. Though we use a small-molecule model in this work, we anticipate that the results presented in this paper may guide experimental work on homogeneously-dispersed, bulk, earth-abundant mixed-metal oxide systems (e.g. perovskites, oxide alloys of Fe/Co/Ni, etc.). We first compute the overpotentials associated with different mechanisms on the same catalysts. Based on previous studies<sup>50</sup>, we point out that it may be possible to predict catalytic overpotentials based on incorrect mechanisms whose rate-determining step (RDS) is chemically similar to the true RDS. We next aim to develop a catalytic screen for mixed alloys of transition metals by studying in detail the properties of mixed metal-oxide dimers, or 'heterobimetallics.' Through the development of this screen, we necessarily must critically examine the utility of the widely-used Sabatier analysis to study the properties of alloys, as its utility in such complex chemical systems is unclear. We find that the electronic interactions between two metals in a dimer is often highly nontrivial, suggesting that one cannot reliably predict the property of heterobimetallic OER catalysts solely from the properties of homobimetallics.

## Computational model

Our goal in this work is to screen a large number of metal-oxide alloys; to reduce the cost of our calculations, we chose to reduce a bulk metal-oxide down to a two-metal small-molecule catalyst, as depicted in Figure 2. The model was chosen to allow us to examine how two transition metals (like or dislike) interact during the course of the mechanisms in Figure 1. The metals have octahedral oxygen coordination sphere (like in most bulk metal oxides), and the ligands were chosen to give the metals the correct oxidation state ( $M^{III}$  for both metals in the depicted intermediate) based on ligands studied in Refs. 51 and 52. The catalytic intermediate can be changed by permuting the protonation state of the two OH ligands bound to the top of the metals, allowing us to study the entire catalytic cycle. With our model, we make the implicit assumption that only nearest-neighbor effects influence catalytic overpotentials.

We computed redox potentials following the procedure detailed in Reference 50; only the broad strokes of the procedure will be outlined here. All *ab initio* calculations were performed using

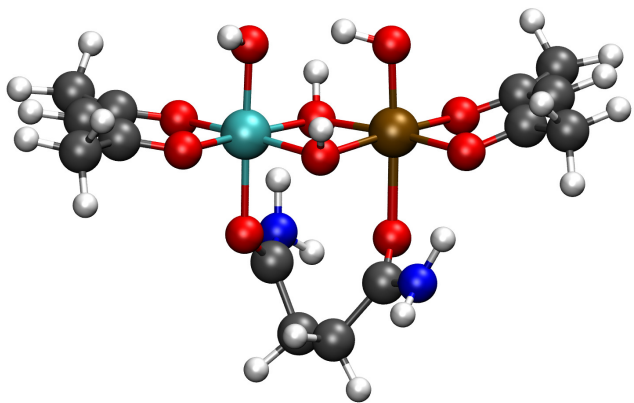


Figure 2: All calculations were performed using the above model complex (White: Hydrogen; Gray: Carbon; Red: Oxygen; Blue: Nitrogen; Cyan and Brown: Transition Metals). This complex was chosen so as to (1) replicate the octahedral oxygen coordination sphere found in heterogeneous metal-oxide catalysts, and (2) fix the oxidation states of each metal. The metal oxidation states are controlled by removing a hydrogen atom (proton + electron) from the simulation on the two apical sites. In this catalytic intermediate, each metal has an -OH at its active site, meaning each metal is in the +3 oxidation state.

PBE0<sup>53</sup> and the 6-31g\* basis set. Geometry optimizations were performed for each intermediate in the catalytic cycle. A stability analysis was performed after each optimization to ensure the structure was at a minimum; imaginary frequencies smaller than  $100\text{ cm}^{-1}$  were assumed to arise from numerical imprecision commonplace in many DFT codes, and their presence led to errors significantly smaller than the standard DFT error.<sup>54</sup> The energy at each minimum was corrected using (1) finite temperature enthalpy corrections, and (2) vibrational entropy corrections, using a combination of the real vibrational frequencies of the intermediate (scaled appropriately for PBE0/6-31g\*<sup>55</sup>) and the equipartition theorem. A solvation correction was also added to the energy, using the polarizable continuum model (PCM)<sup>56,57</sup> with a dielectric of 78.39. A discussion on the use of implicit solvent models for thermochemistry can be found in References 58 and 59.

In order to simplify our analysis, we assumed that the resting state of the catalyst was always M-OH, and the metal in the catalytic resting state had an oxidation state consistent with the metal’s most-prevalent oxidation states (III for most metals, IV for V and Cr). As the catalyst progressed through the catalytic cycle, we adjusted the oxidation accordingly—from III for M-OH and M-OOH, to IV for M-O and M-OO, to II for M-OH<sub>2</sub>. We additionally made the simplifying assumption that each metal had a spin state consistent with a low-spin octahedral crystal field



picture, and that the spins of the two metals in the dimer were ferromagnetically coupled.

We explicitly computed the redox potentials versus the standard hydrogen electrode (SHE) (and, in cases of chemical steps where there was no electron transfer, the  $\Delta G_{rxn}^\circ$ ) for each step in the mechanisms shown in Figure 1. To be consistent with analyses done by other authors<sup>16</sup>, we combined chemical steps (i.e., ones with no explicit electron transfer) with electrochemical steps (i.e., ones with explicit electron transfer) to reduce each mechanism down to four electrochemical steps. We performed the grouping according to the following heuristic:

- If a chemical step is downhill, assume the previous step is pre-equilibrium; group the chemical step with the previous step
- If a chemical step is uphill, it is rate-determining for the chemical transformation; group it and all other following chemical steps with the next electrochemical step.

With four electrochemical redox potentials present for each mechanism, we computed the overpotential  $\eta$  by taking the largest of these four potentials and subtracting from it the thermodynamic potential for water splitting against the SHE, 1.23 V:

$$\eta = E_{max}^\circ - 1.23 \text{ V}$$

where  $E_{max}^\circ$  is the potential of the largest uphill step in the considered mechanisms.

We note in passing that determining overpotentials strictly from thermodynamic data ignores activation barriers. A more rigorous analysis would use transition state energies in the determination of overpotentials; however, in this manuscript, in line with the common practice in the field, we assume that all redox reactions are barrierless, and use the fact that transition state energies cannot be less than intermediate energies.

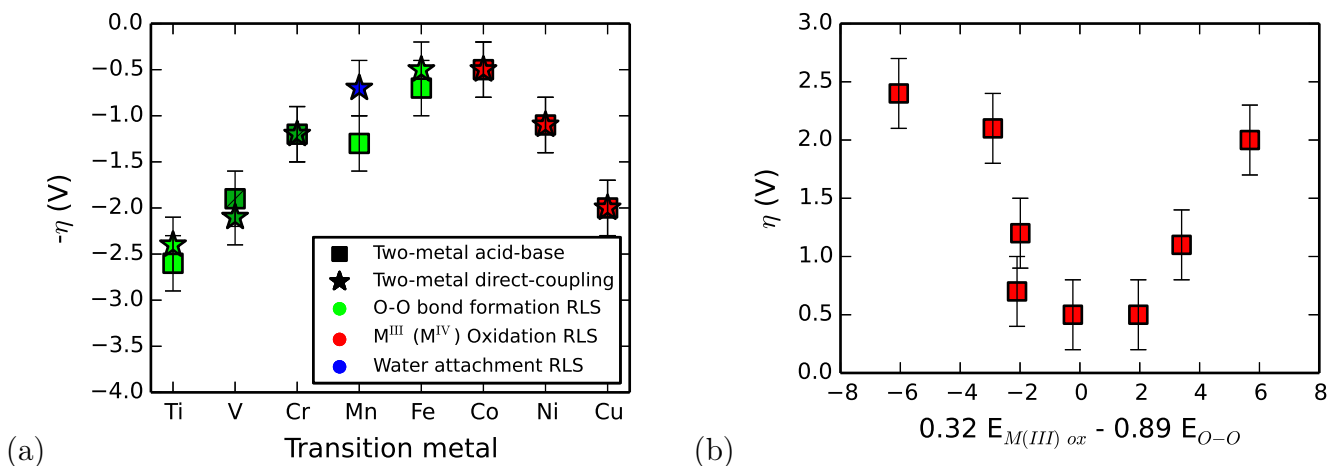


Figure 3: (a) Overpotentials of metal-oxide model clusters follow the expected periodic trend: as the d-orbitals fill up and the number of unpaired  $e_g$  electrons is maximized, the overpotential decreases. This is associated with a change in the mechanistic rate-determining step from O-O bond formation to metal oxidation. Somewhat surprisingly, mechanisms with chemically-similar rate-determining steps have computationally indistinguishable overpotentials, suggesting that DFT can predict overpotentials even if the assumed mechanism is incorrect (but chemically similar to the true mechanism). (b) A principle component analysis of the data used to generate (a) reveals that the coordinate along which the catalytic activity is maximized is a linear combination of the energy of  $M^{III}$  ( $M^{IV}$ ) oxidation and oxygen-oxygen bond formation.

## Results

### Homobimetallic complexes

We begin our search for universal design principles with a scan of the first period of the transition metal series. Figure 3(a) shows the result of this scan. As we go from left to right across the period, the overpotential required to evolve oxygen from a metal-oxide catalyst first decreases, and then increases again—forming a peak in activity consistent with previous experimental and theoretical results<sup>9,18,23,40</sup>. The rate-determining step changes from O-O bond formation on the left side of the period, to  $M^{III}$  oxidation on the right side of the period; this observation is consistent with arguments regarding the origin of this periodic trend based on metal-oxygen bond strength and d-band filling as outlined in detail in the Introduction.

Interestingly, to within error, both mechanisms, acid-base and direct-coupling, predict the same overpotentials. This is consistent with previous literature on the study of OER in rubidium dimers, where experimental<sup>60</sup> and computational<sup>61</sup> evidence have suggested that the acid-base mechanism

dominates for certain sets of ligands but that under different conditions<sup>62–64</sup>, the direct-coupling mechanism may prevail. Our results suggest that mechanisms which share chemically-similar rate-determining steps can give rise to similar overpotentials, even if the mechanism itself is incorrect—confirming our earlier hypothesis. Additionally, this gives a limited justification to the descriptor idea: we show that for homobimetallics, the same descriptors could work for multiple mechanisms. For the remainder of this work, we will thus focus only on direct-coupling overpotentials for simplicity.

We performed a principle component analysis on the six free energy changes associated with the direct coupling mechanism across the metal series in order to better understand the origin of the periodic trend; the result of this analysis is shown in Figure 3(b). Unsurprisingly, the two potentials that best characterize the data are the potential for  $M^{III}$  oxidation (or  $M^{IV}$  oxidation in the case of V/Cr) and the energy for oxygen-oxygen bond formation. For at least the homobimetallic case, where the catalyst is comprised of only a single type of metal, a linear combination of these two energies can serve as an adequate chemical descriptor of catalytic activity.

## Heterobimetallic complexes

Building off of the observed trends for homobimetallic complexes, we extended our investigation to heterobimetallic complexes—catalysts where two different metals can interact, altering the stability of mechanistic intermediates. We note that both metals in the compounds studied here are anticipated to be catalytically active. This is in contrast to certain classes of polymetallic alloys (e.g. perovskites), where even though there are many metals, only one is expected to be catalytically active. To extract general catalytic design principles, we must ask: How does mixing a metal-oxide with a different type of metal affect the energetics of catalysts? And how much of the properties of the heterobimetallic species can be predicted *a priori* from the homobimetallic data?

To answer these questions, we first extended the analysis presented in Figure 3 to metal dimers composed of all possible combinations of metals in the first period of the transition metal series. The overpotentials associated with these dimers are presented in Figure 4. We limit the scope of

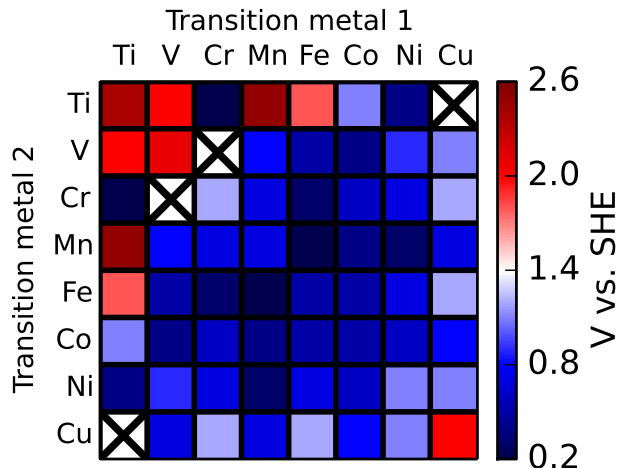


Figure 4: Absolute overpotentials of all heterobimetallic complexes studied, in volts with respect to the standard hydrogen electrode. No data is reported for two complexes, Ti-Cu and V-Cr, as certain catalytic intermediates in each case fell apart upon geometry optimization. Additionally, Cr-Mn through Cr-Ni complexes did not remain octahedral during O-O bond formation, and Mn-Cu was found to have a different resting state ( $\text{Mn-O-Cu-OH}_2$ ) than the other complexes studied. Certain heterobimetallic combinations have lower overpotentials than any homobimetallic, suggesting an axis along which catalytic activity can be optimized.

our discussion for the heterobimetallics to the direct coupling mechanism. The diagonal elements of the pictured overpotential matrix are the direct coupling overpotentials depicted in Figure 3.

Of greater interest are the off-diagonal elements, which represent heterodimer overpotentials. Some of these have lower overpotentials than the homobimetallic materials, that might lead to higher catalytic turnover; additionally, some of these heterobimetallics have overpotentials that are much lower than expected. One example in the Ni-Mn heterodimer, which has a predicted overpotential lower than that of either the Ni-Ni or the Mn-Mn homodimer. Of the screened materials with small overpotentials, we suspect that Ti-Cr and Ti-Ni may be questionable, as titanium(III) oxide catalysts are known to be inefficient due to their large band gaps<sup>65</sup>. Additionally, many of the chromium dimers required a significant distortion of the ligand field in order to accommodate O-O bond formation. These materials aside, none of the rest of the materials screened showed any large issues, so we expect the overpotentials of materials containing Mn-, Fe-, Co- and Ni- to be chemically relevant—to within the accuracy of our DFT calculations. We are unable to, e.g., order the overpotentials of Ni-Fe, Ni-Co, and Co-Fe with respect to one another, because they are all the same to within the error of our calculations; the ordering presented here

may thus be inconsistent with experimental observations<sup>66</sup>.

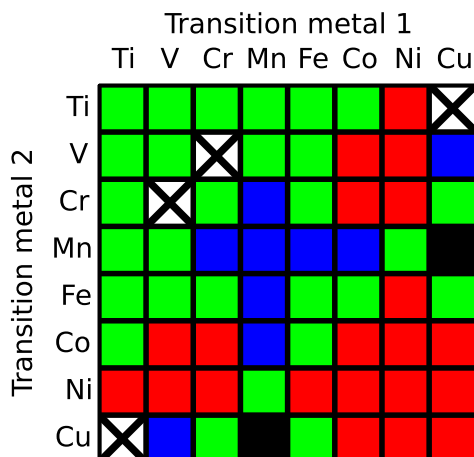


Figure 5: Rate-determining steps of the oxygen evolution reaction on transition metal-oxide dimers. While the homobimetallics showed a clear trend, the RDS of heterobimetallic species is much more varied. A Sabatier analysis thus cannot be applied in a straightforward manner to the heterobimetallics.

To understand the origins of the overpotentials presented in Figure 4, we examine qualitatively which step in the water splitting cycle is the rate-determining step. The results are presented in Figure 5. While the mechanism of homobimetallic complexes (see Figure 3) shows a clear trend—shifting from an O-O bond formation RDS to a metal oxidation RDS across the period—the corresponding analysis of the RDS of heterobimetallic complex does no such thing. O-O bond formation is the predominant RDS: it accounts for the bottleneck step in over half of the complexes studied.

To better understand the character of the RDS in heterobimetallic complexes, we computed the Mulliken spin populations of the terminal oxygen atoms in the  $M=O$   $M=O$  intermediates. What we found was interesting, but not unexpected: Generally speaking, for heterobimetallics where O-O bond formation is the RDS, at least one  $M=O$  oxygen has a spin population very closer to zero, indicating little to no oxygen radical character. Conversely, for heterobimetallics where another step (such as metal oxidation) is the RDS, both  $M=O$  oxygens have significant radical character. This makes sense: Since O-O bond formation in the radical-coupling mechanism involves the sharing of electrons between two oxygen atoms, O-O bond formation should be very low in energy compared to other steps in the cycle if both oxygens have significant radical character.

In spite of this observation, nickel-containing complexes have a tendency to have metal oxidation as the RDS, and manganese-containing complexes water attachment. Because of these frequent blips, a Sabatier analysis is not straightforward; we will thus focus our discussion on trying to understand the origin of these trends and searching for a descriptor that can be used to inform catalytic design.

## Discussion

### Metal Cooperativity

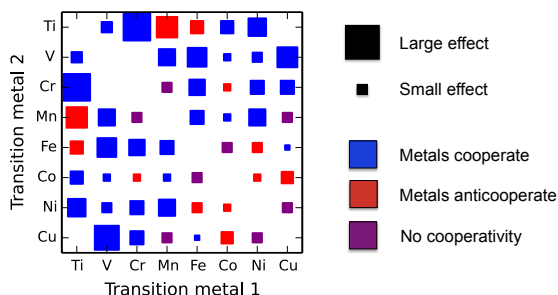


Figure 6: For each metal pair, we compute a naive estimation of the overpotential by taking either (1) the homobimetallic overpotential of the site associated with the chemistry of the RDS, or (2) the average of the two homobimetallic overpotentials for the alloy in question if the RDS is O-O bond formation. By plotting the difference between the heterobimetallic overpotential and our naive estimate, we extract a measure of how cooperative the metals are in the heterodimers. Blue squares represent a positive effect (i.e. the metals work together to lower overpotentials) and red squares represent a negative effect. The size of the square corresponds to the magnitude of the effect.

We recapitulate that our desire in this work is to understand how much of the properties of the heterobimetallics can be predicted solely from the properties of the homobimetallics, and how a mapping of one on to the other can inform rational design. We begin our analysis by quantifying how much two unlike metals cooperate with one another to lower overpotentials. With the exception of O-O bond formation, each step in the direct-coupling mechanism is local: it occurs on only one of the two metals in the complex. As a measure of cooperativity, then, we ask: for a RDS occurring primarily on metal A in the transition metal dimer A-B, what is the difference between the A-B overpotential and the A-A overpotential? Or, in the case where the RDS is O-O

bond formation, what is the difference between the A-B overpotential with the average of the A-A and B-B overpotentials?

Figure 6 shows the results of this analysis. We observe, generally, that in the lower-right corner of the table—where metal(III) oxidation is the RDS—metal dimers tend to behave weakly anti-cooperatively or independently. In the region near Mn-Mn—where water attachment is the RDS—metal dimers tend to behave weakly cooperatively or independently. By contrast, in the rest of the table—where O-O bond formation is the RDS—metal dimers tend to cooperate strongly.

These observations are consistent with our chemical intuition that when chemistry is local (i.e. the RDS only involves one metal site directly), the other metal center tends to act as a spectator, only weakly influencing the RDS. We point out an exception to this rule in the case of creating alloys with Ni (where the RDS is predominantly metal(III) / metal(IV) oxidation but we observe strong cooperativity). This exception can be understood by examining the individual redox potentials for Ni oxidation versus M oxidation for each other metal in the series, as plotted in Figure 7. The RDS in this series does actually change from Ni oxidation to M oxidation across the period. This change in RDS inflates our cooperativity metric towards the left half of this series, as overpotentials are being drastically lowered by changing the RDS from O-O bond formation to Ni oxidation.

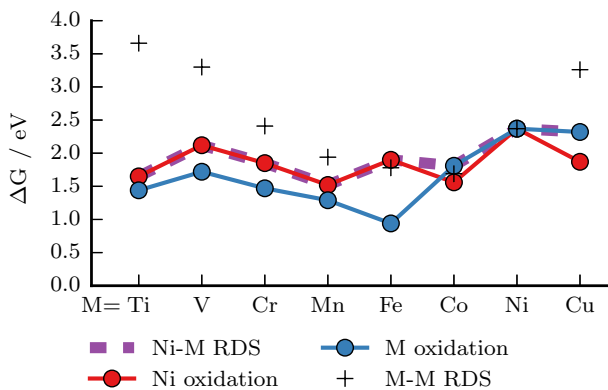


Figure 7: Examining Ni-M dimers across the series of metals reveals an interesting trend: overpotentials of Ni-M species are generally lowered with respect to M-M species because the O-O bond formation energy is substantially lowered, making a metal oxidation event the rate-determining step. For the first half of the series, Ni oxidation is higher in energy than M oxidation, making it the RDS; later, this flips, and M oxidation becomes the RDS.

O-O bond formation, on the other hand, is inherently nonlocal, and thus requires more than

the sum of its parts. Interestingly, in this case, we observe that overpotentials on heterodimers which arise due to large barriers for O-O bond formation are reduced significantly compared to the average of the homodimer overpotentials, indicating non-equal contributions from the two metals in the radical coupling step. Overall, the results in Figure 6 tell us how many of the overpotentials presented in Figure 4 could have been guessed looking only at the overpotentials in Figure 3. In cases where cooperativity is small, homobimetal overpotentials are a good predictor of alloy overpotentials; in cases where cooperativity is large, they are not a good predictor. Thus, we must continue our search for a good universal predictor of alloy catalytic activity.

## Metal Communication

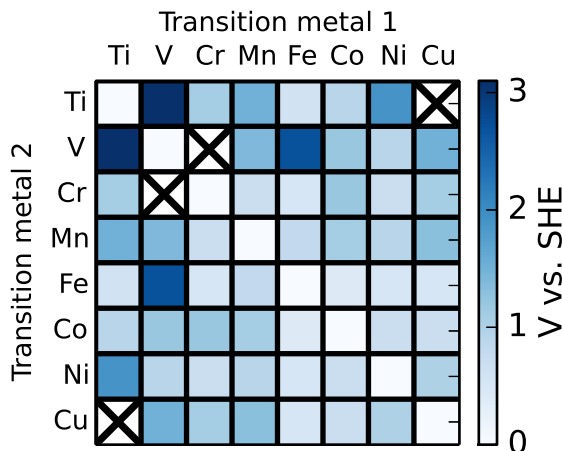


Figure 8: We wish to determine whether or not any information about heterodimer overpotentials can be surmised by looking at only the homodimer data. For each heterodimer, we constructed a series of 6 chemical and electrochemical energies / redox potentials assuming the metals do not interact (except for O-O bond formation, where they interact in a mean-field sense). Concretely, we took the lower of the two homodimer energies for the two steps where there is a choice to be made (the initial metal oxidation, and the site of water attachment), and followed the chemistry of the mechanism through for the rest of the energies. The RMSD of these six energies from the heterodimer energies is shown, where the homodimers by definition have an RMSD of 0 V.

We next ask the question: Is an *a priori* universal predictor of heterobimetallic activity even possible, or do the metals interact to such a significant effect that finding such a descriptor is hopeless? We address this question by measuring *communication* between the metals. As a metric for communication, we must look not only at how much the redox potential of the RDS



changes going from a homobimetal-based description of redox potentials to a heterobimetal-based description, but also at how much *every* redox potential changes.

For this analysis, we use all six free energy changes occurring in the direct coupling cycle presented in Figure 1, as combining chemical and electrochemical steps obfuscates metal communication. For each metal pair, we look at the two sets of homobimetal redox potentials (and free energy changes) for the two metals in the heterodimer. We compute six naive overpotentials for the heterodimer using the following procedure:

1. First metal oxidation is the lower of the two homodimer metal oxidation potentials
2. If the first oxidation occurred on the left metal, take the second metal oxidation potential from the right metal, or vice-versa
3. Average the two homodimer O-O bond formation free energies
4. Take the lower of the two homodimer free energies for water attachment
5. If water attachment occurred on the left metal, take the third redox potential from the left metal, or vice-versa
6. If water attachment occurred on the left metal, take the final redox potential from the right metal, or vice-versa.

These six redox potentials (and free energies) form a naive picture of the thermodynamics of catalysis on a heterodimer: If the metals do not communicate much or at all, we would expect the true heterodimer potentials / energies to be very close to these naive potentials / energies; if the metals communicate a lot, we would expect the true heterodimer energies to deviate substantially from the naive energies.

We measure the root-mean-square deviation (RMSD) of the true redox potentials from the naive redox potentials of all six steps for each metal dimer; the results are plotted in Figure 8. We wish to make two observations about the data. First, overall, most of the metals in the heterodimers communicate fairly substantially; in all of our data, the smallest RMSD is 0.4 V (for Co-Fe) and the largest is 3.1 V (for Ti-V), and the mean RMSD is 0.9 V. Second, the communication data

show only a weak correlation with the cooperativity data in Figure 6. We observe that when the RDS is metal oxidation or water attachment, the metals on average communicate less than when the RDS is O-O bond formation (again, consistent with our chemical intuition); any deeper insights are difficult to perceive.

From these observations, we conclude that even if metals communicate, it isn’t necessarily in a way that affects cooperativity—sometimes, communication just affects redox potentials that aren’t the RDS. While this indirectly affects overpotentials (as raising the potential of one step necessarily lowers the energy of at least one other), it does not necessitate the lowering of overpotentials. We can additionally conclude that while there is overall a lot of metal-metal communication, since it does not necessarily affect the RDS, it should (in principle) be possible to extract descriptors of catalytic activity from the data.

## Sabatier Analysis

Given the complexity of all that we’ve discussed so far, we return to our original questions: Does the Sabatier analysis break down due to the large amounts of communication and cooperativity in certain metal pairs? And can we use anything we know about homobimetals help predict heterobimetal behavior? To answer the first of these questions (and help us answer the second), we perform a principle component analysis on the data<sup>67</sup>—again using all six free energy changes implicated in the direct coupling catalytic cycle instead of folding chemical steps into electrochemical steps as discussed previously. Principle component analyses of a swath of redox potentials have been performed previously for the oxygen reduction reaction with successful experimental implications<sup>68,69</sup>.

The results of our principle component analysis are shown in Figure 9. The principle eigenvector of the covariance matrix of redox potentials (averaged over the ensemble of all metal pairs) is, in full,

$$e_1 = 0.32E_{M(III)_{ox1}} + 0.20E_{M(III)_{ox2}} - 0.89E_{O-O} + 0.20E_{H_2O_{add}} + 0.18E_{M(II)_{ox}}$$

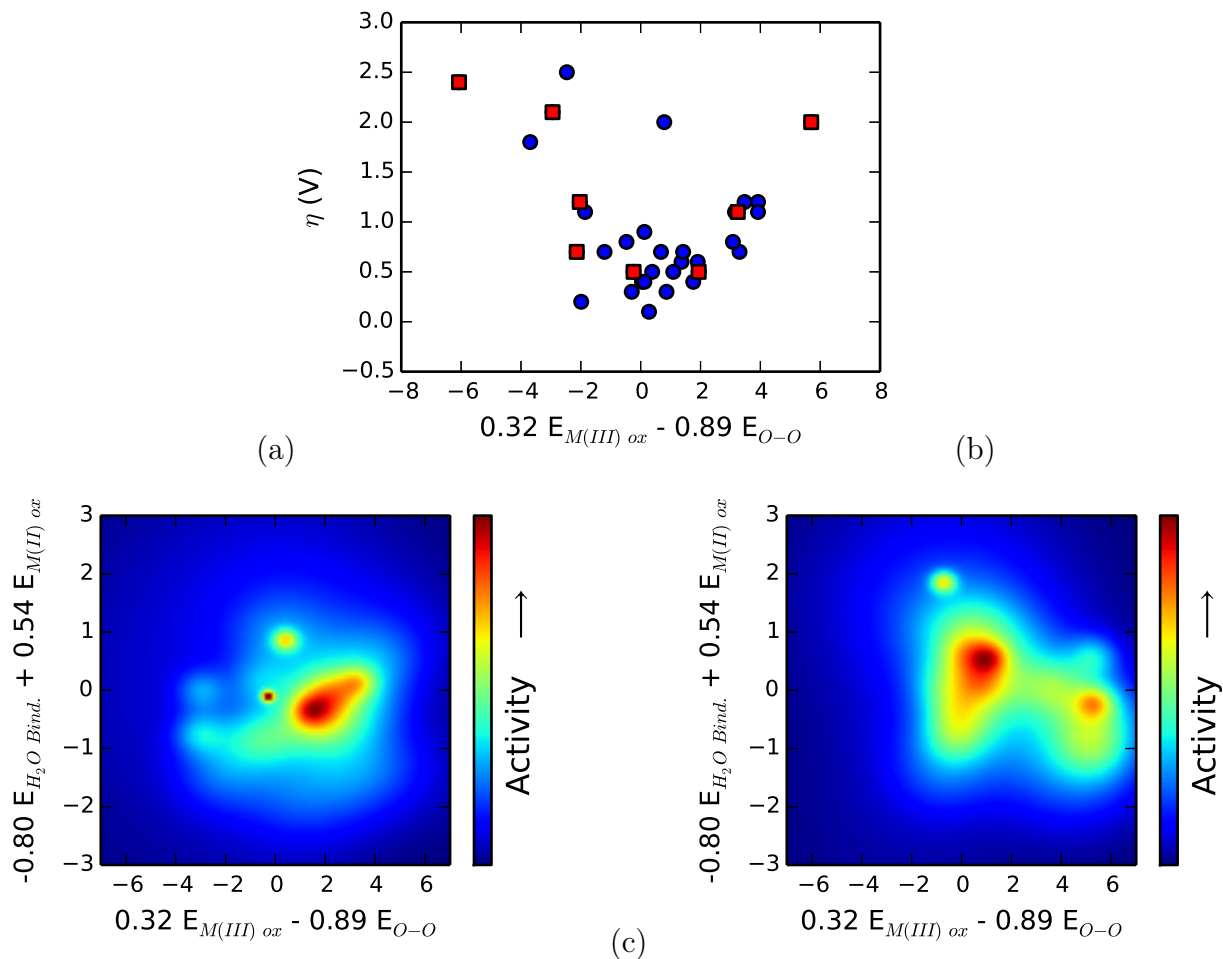


Figure 9: A principle component analysis of the six free energy differences computed for all compounds studied reveals two key coordinates which can be used as descriptors of catalytic activity. (a) Examining only the first of these two coordinates does not conclusively show a peak in activity, as the data has lots of scatter (especially once the homobimetallic points, pictured as red squares, are excised from the data). (b) Looking at both coordinates reveals a clear volcanic island of activity. (c) To see whether or not heterobimetal activities can be predicted using homobimetal data, we took the appropriate linear combinations of our “naive” heterobimetallic redox potentials (i.e. redox potentials predicted using only the homobimetallic data; the same set as used in Figure 8) and correlated it with activity.

which accounts for 74.1% of the spread of the data. This coordinate can be approximated by its two largest values,

$$e_1 \approx 0.32E_{M(III)ox1} - 0.89E_{O-O}$$

Plotted versus this linear combination of potentials, the traditional Sabatier analysis breaks down (Figure 9(a)). While there is a volcano-like envelope of 'ideal' cases where this coordinate is a successful predictor of overpotential, there is also a large amount of scatter in the data, meaning there are even more cases where the coordinate does not successfully predict overpotentials. This is especially true if the homobimetallic data are excised.

We do, however, recover Sabatier-like behavior if the second eigenvector (which accounts for an additional 14.5% of the variance of the data) is included; in full, this eigenvector is

$$e_1 = 0.25E_{M(III)ox2} - 0.80E_{H_2O\ add} + 0.54E_{M(II)ox}$$

which can again be approximated by its two largest components,

$$e_2 \approx -0.80E_{H_2O\ add} + 0.54E_{M(II)ox}$$

The correlation of overpotential with these two coordinates is shown in Figure 9(b). A volcano of activity emerges along these two coordinates where none existed along only the first. Additionally, each other eigenvector of the covariance matrix accounts for no more than 6.2% of the variance, suggesting that only the two coordinates presented are chemically relevant for exploring design space. We thus conclude that we cannot use a single chemical descriptor to screen heterobimetallic catalysts; our data suggest that at least two descriptors are required.

Based on these central results, one might suppose that a descriptor of catalytic activity could be attained by using the above generalized coordinates. An attractive prospect emerges: Computation of the M(II) and M(III) ionization potentials and M-OH<sub>2</sub> bond enthalpies for two independent metal-oxide catalysts may be able to provide a reasonable stand-in for the same energies in an

alloy, as each corresponds to an event that occurs relatively locally on a single metal. The O-O bond formation energy may also be naively estimated as an average of the O-O bond formation energies for two homodimers. We thus conclude by returning to the central question of this manuscript: Can we predict the overpotentials of metal oxide alloys by only looking at properties of individual metal oxides?

To answer this question, we plot the computed activities of the heterobimetallic catalysts as functions of linear combinations of *homobimetallic* redox potentials. For each heterobimetallic, we choose the “best” homobimetallic potential for each step using the procedure described earlier; the linear combinations are the two primary principle components described above.

The result is shown in Figure 9(c). As can be seen, the resulting ‘predicted’ 2d volcano plot is dissimilar to the ‘actual’ 2d volcano, showing that even with careful analysis, one cannot readily predict the overpotentials of heterobimetallics using only homobimetallic data. This result is consistent with our earlier analysis: the metals tend to communicate and cooperate when the RDS is O-O bond formation, which is the majority of cases, suggesting that for these systems catalysis is truly a complex, two-center process that is more than the sum of its parts.

## Conclusions

A pure computational screen based on a single chemical descriptor, or a pure Sabatier analysis based on periodic trends of reactivity, cannot describe the rich redox behavior observed in the heterobimetallics. In this manuscript, we have presented a more detailed analysis of the redox activity of transition metal dimers. We have shown that predicting the true mechanism of OER is not necessary to accurately predict overpotentials if a mechanism with a chemically-similar RDS is considered instead. We additionally showed that while a Sabatier analysis holds for the case of homobimetallic species, a more nuanced treatment is required to tease out trends in activity among the heterobimetallics; this nuanced treatment, in turn, cannot be used to predict heterobimetal overpotential from homobimetal data.

In this paper, we have shown with a model system that at least in some cases, the descriptor picture works well when there’s only one metal, but can break down when multiple are involved

in the redox chemistry. Nonetheless, Sabatier analysis has been successfully applied to predict activities of a plethora of catalysts which have been experimentally realized<sup>9,70,71</sup>. A descriptor picture is more likely to be accurate when catalysis either occurs primarily on a single metal center, or occurs via a two-center mechanism that has a rate-determining step that is chemically similar to a one-center step. In more complex cases, such as where the RDS of catalysis inherently involves two metal centers, a naive Sabatier analysis oversimplified the actual activity trends.

As our analysis shows, there are chemical descriptors that can be had both when catalysis is simple and when it is complex; in the latter case, the descriptors are simply more subtle and detailed than one might hope. Thus, there is hope that the existing Sabatier analyses may have produced some false negatives, ruling out catalysts that work very well but buck simple trends. A re-doubling of both experimental and theoretical effort on previously studied complex OER systems may be warranted.

We conclude by laying out a roadmap for a more comprehensive approach to studying OER catalysis. We limited our analysis in this work to small-molecule first-row metal dimers in octahedral coordination geometries with a very particular selection of oxidation and spin states. Moving forward, questions of realism are central: important considerations in surface chemistry, including morphology, surface stability, and longevity in the presence of an polarizing electrode, may influence redox potentials substantially.

Additionally, the effect of mechanism on observed overpotential is still open. Alternative mechanisms which are chemically dissimilar from those studied, such as those involving intramolecular proton-coupled electron transfer (or just proton transfer), have been shown to potentially alter observed overpotentials<sup>72,73</sup>. Also, mechanism switching between acid-base and direct-coupling across a period may occur. While we do not expect this to dramatically affect overpotentials (spurred by the results shown in Figure 3), further investigation may be warranted.

Finally, differences in solid state (or extended) systems effects may be substantial, as indicated by the significant average communication between metal centers reported in Figure 8. Further computational studies are needed to determine the extent of metal-metal communication in an alloy.

To study these problem, more accurate (yet still fast) computation of redox potentials are required as the phenomena under scrutiny become more and more complex. We have recently developed a means to compute redox potentials with near-QMMM accuracy at a fraction of the cost<sup>74</sup>. Application of this method to some of the problems raised will help further the understanding of OER catalysis and ultimately improve criteria for rational design.

**Supporting Information.** Geometries (.xyz file format), final SCF energies, and imaginary frequencies of all dimers studied in this manuscript can be found in the Supporting Information. Additionally, Mulliken charges and spin populations of the metals and terminal oxygen atoms in the M=O M=O compounds can be found in the Supporting Information.

**Acknowledgement.** M. G. M. would like to acknowledge Yang Shao-Horn, Marcel Risch, Yogi Surendranath, Kwabena Bediako, and Andrew Ullman for helpful discussions, as well as the NSF Graduate Research Fellowship Program for funding. This work was supported by NSF CHE-1464804.

## References

- (1) McEvoy, J. P.; Gascon, J. A.; Batista, V. S.; Brudvig, G. W. The Mechanism of Photosynthetic Water Splitting. *Photoch. Photobio. Sci.* **2005**, *4*, 940–949.
- (2) McEvoy, J. P.; Brudvig, G. W. Water-Splitting Chemistry of Photosystem II. *Chem. Rev.* **2006**, *106*, 4455–4483.
- (3) Sproviero, E. M.; Gascón, J. A.; McEvoy, J. P.; Brudvig, G. W.; Batista, V. S. Quantum Mechanics/Molecular Mechanics Study of the Catalytic Cycle of Water Splitting in Photosystem II. *J. Am. Chem. Soc.* **2008**, *130*, 3428–3442.
- (4) Kudo, A.; Miseki, Y. Heterogeneous Photocatalyst Materials for Water Splitting. *Chem. Soc. Rev.* **2009**, *38*, 253–278.
- (5) Nocera, D. G. The Artificial Leaf. *Acc. Chem. Res.* **2012**, *45*, 767–776.

- (6) Concepcion, J. J.; Jurss, J. W.; Templeton, J. L.; Meyer, T. J. One Site Is Enough. Catalytic Water Oxidation by  $[\text{Ru}(\text{tpy})(\text{bpm})(\text{OH}_2)]^{2+}$  and  $[\text{Ru}(\text{tpy})(\text{bpz})(\text{OH}_2)]^{2+}$ . *J. Am. Chem. Soc.* **2008**, *130*, 16462–16463.
- (7) Wang, L.-P.; Wu, Q.; Van Voorhis, T. Acid-Base Mechanism for Ruthenium Water Oxidation Catalysts. *Inorg. Chem.* **2010**, *49*, 4543–4553.
- (8) Kanan, M. W.; Nocera, D. G. In Situ Formation of an Oxygen-Evolving Catalyst in Neutral Water Containing Phosphate and  $\text{Co}^{2+}$ . *Science* **2008**, *321*, 1072–5.
- (9) Suntivich, J.; May, K. J.; Gasteiger, H. A.; Goodenough, J. B.; Shao-Horn, Y. A Perovskite Oxide Optimized for Oxygen Evolution Catalysis from Molecular Orbital Principles. *Science* **2011**, *334*, 1383–1385.
- (10) Risch, M.; Klingan, K.; Ringleb, F.; Chernev, P.; Zaharieva, I.; Fischer, A.; Dau, H. Water Oxidation by Electrodeposited Cobalt Oxides—Role of Anions and Redox-Inert Cations in Structure and Function of the Amorphous Catalyst. *ChemSusChem* **2012**, *5*, 542–549.
- (11) Wang, Y.; Cheng, H.-P. Oxygen Reduction Activity on Perovskite Oxide Surfaces: A Comparative First-Principles Study of  $\text{LaMnO}_3$ ,  $\text{LaFeO}_3$ , and  $\text{LaCrO}_3$ . *J. Phys. Chem. C* **2013**, *117*, 2106–2112.
- (12) Hachmann, J.; Olivares-Amaya, R.; Atahan-Evrenk, S.; Amador-Bedolla, C.; Sánchez-Carrera, R. S.; Gold-Parker, A.; Vogt, L.; Brockway, A. M.; Aspuru-Guzik, A. The Harvard Clean Energy Project: Large-Scale Computational Screening and Design of Organic Photovoltaics on the World Community Grid. *J. Phys. Chem. Lett.* **2011**, *2*, 2241–2251.
- (13) Hautier, G.; Fischer, C. C.; Jain, A.; Mueller, T.; Ceder, G. Finding Nature’s Missing Ternary Oxide Compounds Using Machine Learning and Density Functional Theory. *Chem. Mater.* **2010**, *22*, 3762–3767.
- (14) Raccuglia, P.; Elbert, K. C.; Adler, P.; Falk, C.; Wenny, M.; Mollo, A.; Zeller, M.; Friedler, S. A.; Schrier, J.; Norquist, A. Machine-Learning-Assisted Materials Discovery Using Failed Experiments. *Nature* **2016**, *533*, 73–76.



- (15) Sabatier, P. Hydrogénations et Déshydrogénations Par Catalyse. *Ber. Deut. Chem. Ges.* **1911**, *44*, 1984–2001.
- (16) Norskov, J. K.; Rossmeisl, J.; Logadottir, A.; Lindqvist, L.; Kitchin, J. R.; Bligaard, T.; Jónsson, H. Origin of the Overpotential for Oxygen Reduction at a Fuel-Cell Cathode. *J. Phys. Chem. B* **2004**, *108*, 17886–17892.
- (17) Rossmeisl, J.; Logadottir, A.; Norskov, J. K. Electrolysis of Water on (Oxidized) Metal Surfaces. *Chem. Phys.* **2005**, *319*, 178–184.
- (18) Norskov, J. K.; Bligaard, T.; Rossmeisl, J.; Christensen, C. H. Towards the Computational Design of Solid Catalysts. *Nat. Chem.* **2009**, *1*, 37–46.
- (19) Quaino, P.; Juarez, F.; Santos, E.; Schmickler, W. Volcano Plots in Hydrogen Electrocatalysis—Uses and Abuses. *Beilstein J. Nano.* **2014**, *5*, 846–54.
- (20) Zhang, B.; Zheng, X.; Voznyy, O.; Comin, R.; Bajdich, M.; García-melchor, M.; Han, L.; Xu, J.; Liu, M.; Zheng, L. et al. Homogeneously Dispersed, Multimetal Oxygen-Evolving Catalysts. *Science* **2016**, *1525*, 1–11.
- (21) Mo, Y.; Ong, S. P.; Ceder, G. First-Principles Study of the Oxygen Evolution Reaction of Lithium Peroxide in the Lithium-Air Battery. *Phys. Rev. B* **2011**, *84*, 205446.
- (22) Garcia-Mota, M.; Vojvodic, A.; Metiu, H.; Man, I. C.; Su, H. Y.; Rossmeisl, J.; Norskov, J. K. Tailoring the Activity for Oxygen Evolution Electrocatalysis on Rutile TiO<sub>2</sub>(110) by Transition-Metal Substitution. *ChemCatChem* **2011**, *3*, 1607–1611.
- (23) Man, I. C.; Su, H.-Y.; Calle-Vallejo, F.; Hansen, H. A.; Martínez, J. I.; Inoglu, N. G.; Kitchin, J.; Jaramillo, T. F.; Norskov, J. K.; Rossmeisl, J. Universality in Oxygen Evolution Electrocatalysis on Oxide Surfaces. *ChemCatChem* **2011**, *3*, 1159–1165.
- (24) Boero, M.; Parrinello, M.; Weiss, H.; Huffer, S. A First Principles Exploration of a Variety of Active Surfaces and Catalytic Sites in Ziegler-Natta Heterogenous Catalysis. *J. Phys. Chem. A* **2001**, *105*, 5096–5105.

- (25) Greeley, J.; Jaramillo, T. F.; Bonde, J.; Chorkendorff, I. B.; Norskov, J. K. Computational High-Throughput Screening of Electrocatalytic Materials for Hydrogen Evolution. *Nat. Mater.* **2006**, *5*, 909–13.
- (26) Chrétien, S.; Metiu, H. Density Functional Study of the CO Oxidation on a Doped Rutile TiO<sub>2</sub>(110): Effect of Ionic Au in Catalysis. *Catal. Lett.* **2006**, *107*, 143–147.
- (27) Diego, S.; Carter, L. D.; Pease, V. L.; Hillhouse, J. W.; Andersen, O. G. N.; Herman, Y.; Stroeve, J.; Holland, M. M.; Meier, W.; Scambos, T. et al. Identification of Non-Precious Metal Alloy Catalysts for Selective Hydrogenation of Acetylene. *Science* **2008**, *320*, 1320–1322.
- (28) Ceder, G.; Hauthier, G.; Jain, A.; Ong, S. P. Recharging Lithium Battery Research with First-Principles Methods. *Mater. Res. Soc. Bull.* **2011**, *36*, 185–191.
- (29) Curtarolo, S.; Hart, G. L. W.; Nardelli, M. B.; Mingo, N.; Sanvito, S.; Levy, O. The High-Throughput Highway to Computational Materials Design. *Nat. Mater.* **2013**, *12*, 191–201.
- (30) Yu, L.; Zunger, A. Identification of Potential Photovoltaic Absorbers Based on First-Principles Spectroscopic Screening of Materials. *Phys. Rev. Lett.* **2012**, *108*, 068701.
- (31) Bockris, J. O.; Otagawa, T. Mechanism of Oxygen Evolution on Perovskites. *J. Phys. Chem.* **1983**, *87*, 2960–2971.
- (32) Ruetschi, P.; Delahay, P. Influence of Electrode Material on Oxygen Overvoltage—A Theoretical Analysis. *J. Chem. Phys.* **1955**, *23*, 556–560.
- (33) Rossmeisl, J.; Qu, Z. W.; Zhu, H.; Kroes, G. J.; Norskov, J. K. Electrolysis of Water on Oxide Surfaces. *J. Electroanal. Chem.* **2007**, *607*, 83–89.
- (34) Vojvodic, A.; Norskov, J. K. Optimizing Perovskites for the Water-Splitting Reaction. *Science* **2011**, *334*, 1355–1356.
- (35) Betley, T. A.; Wu, Q.; Van Voorhis, T.; Nocera, D. G. Electronic Design Criteria for O-O Bond Formation Via Metal-Oxo Complexes. *Inorg. Chem.* **2008**, *47*, 1849–61.

- (36) Hansen, H. A.; Viswanathan, V.; Norskov, J. K. Unifying Kinetic and Thermodynamic Analysis of  $2e^-$  and  $4e^-$  Reduction of Oxygen on Metal Surfaces. *J. Phys. Chem. C* **2014**, *118*, 6706–6718.
- (37) Sheppard, D.; Henkelman, G.; Von Lilienfeld, O. A. Alchemical Derivatives of Reaction Energetics. *J. Chem. Phys.* **2010**, *133*, 084104.
- (38) Bork, N.; Bonanos, N.; Rossmeisl, J.; Vegge, T. Simple Descriptors for Proton-Conducting Perovskites from Density Functional Theory. *Phys. Rev. B* **2010**, *82*, 1–6.
- (39) Oberhofer, H.; Reuter, K. First-Principles Thermodynamic Screening Approach to Photocatalytic Water Splitting with Co-Catalysts. *J. Chem. Phys.* **2013**, *139*, 044710.
- (40) Suntivich, J.; Gasteiger, H. A.; Yabuuchi, N.; Nakanishi, H.; Goodenough, J. B.; Shao-Horn, Y. Design Principles for Oxygen-Reduction Activity on Perovskite Oxide Catalysts for Fuel Cells and Metal-Air Batteries. *Nat. Chem.* **2011**, *3*, 546–50.
- (41) Trasatti, S. Electrocatalysis by Oxides—Attempt at a Unifying Approach. *J. Electroanal. Chem.* **1980**, *111*, 125–131.
- (42) Joya, K. S.; de Groot, H. J. M. Biomimetic Molecular Water Splitting Catalysts for Hydrogen Generation. *Int. J. Hydrogen Energ.* **2012**, *37*, 8787–8799.
- (43) Tagore, R.; Crabtree, R. H.; Brudvig, G. W. Oxygen Evolution Catalysis by a Dimanganese Complex and Its Relation to Photosynthetic Water Oxidation. *Inorg. Chem.* **2008**, *47*, 1815–1823.
- (44) Surendranath, Y.; Kanan, M. W.; Nocera, D. G. Mechanistic Studies of the Oxygen Evolution Reaction by a Cobalt-Phosphate Catalyst at Neutral pH. *J. Am. Chem. Soc.* **2010**, *132*, 16501–16509.
- (45) Wang, L.-P.; Van Voorhis, T. Direct-Coupling  $O_2$  Bond Forming a Pathway in Cobalt Oxide Water Oxidation Catalysts. *J. Phys. Chem. Lett.* **2011**, *2*, 2200–2204.

- (46) Bediako, D. K.; Surendranath, Y.; Nocera, D. G. Mechanistic Studies of the Oxygen Evolution Reaction Mediated by a Nickel-Borate Thin Film Electrocatalyst. *J. Am. Chem. Soc.* **2013**, *135*, 3662–74.
- (47) Concepcion, J. J.; Tsai, M.-K.; Muckerman, J. T.; Meyer, T. J. Mechanism of Water Oxidation by Single-Site Ruthenium Complex Catalysts. *J. Am. Chem. Soc.* **2010**, *132*, 1545–1557.
- (48) Koper, M. T. M. Thermodynamic Theory of Multi-Electron Transfer Reactions: Implications for Electrocatalysis. *J. Electroanal. Chem.* **2011**, *660*, 254–260.
- (49) Balcells, D. *Adv. Organomet. Chem.*, 1st ed.; Elsevier Inc., 2016; pp 1–59.
- (50) Mavros, M. G.; Tsuchimochi, T.; Kowalczyk, T.; McIsaac, A.; Wang, L.-P.; Van Voorhis, T. What Can Density Functional Theory Tell Us About Artificial Catalytic Water Splitting? *Inorg. Chem.* **2014**, *53*, 6386–6397.
- (51) Coupez, B.; Boehme, C.; Wipff, G. Interaction of Bifunctional Carbonyl and Phosphoryl Ligands with  $M^{3+}$  Lanthanide Cations: How Strong is the Bidentate Effect? The Role of Ligand Size and Counterions Investigated by Quantum Mechanics. *Phys. Chem. Chem. Phys.* **2002**, *4*, 5716 – 5729.
- (52) Willey, G. R.; Baker, R. J.; Haslop, J. V.; Spry, M. P.; Drew, M. G. B. Coordination Studies of the Ligand Series  $RNH\cdot CO\cdot (CH_2)_n\cdot CO\cdot NHR$  Where R=alkyl, Aryl; 0=O, S and n=0,1,2. Part 6. Crystal Structures and Bonding Considerations of the Ligands  $MeNH\cdot CO\cdot CH_2\cdot CO\cdot NHMe$  (L1),  $MeNH\cdot CO\cdot CH_2\cdot CH_2\cdot CO\cdot NHMe$  (L4),  $MeNH\cdot CS\cdot CH_2\cdot CS\cdot NHMe$  (L5) and the  $Sn^{IV}$  Complexes  $SnBr_4L1\cdot L1$ ,  $SnBr_4L2\cdot 2THF$  and  $SnBr_4L3\cdot MeCN$  Where  $L2=iC_3H_7NH\cdot CO\cdot CH_2\cdot CO\cdot NH iC_3H_7$  and  $L3=iC_3H_7NH\cdot CS\cdot CH_2\cdot CS\cdot NH iC_3H_7$ . *Polyhedron* **1998**, *17*, 3291 – 3303.
- (53) Adamo, C.; Barone, V. Toward Reliable Density Functional Methods Without Adjustable Parameters: The PBE0 Model. *J. Chem. Phys.* **1999**, *110*, 6158.
- (54) There were a small number of structures (typically fewer than one per catalytic cycle) that had larger imaginary frequencies. We performed manual testing of these modes, consisting of a

structural perturbation along the eigenvectors corresponding to these frequencies followed by re-optimization. We found that the bridging ligand tended to fall off, reflecting the metastability of the structures found with respect to this type of dissociation. We concluded that further optimization of these structures would not have yielded usable or appreciably-different conclusions.

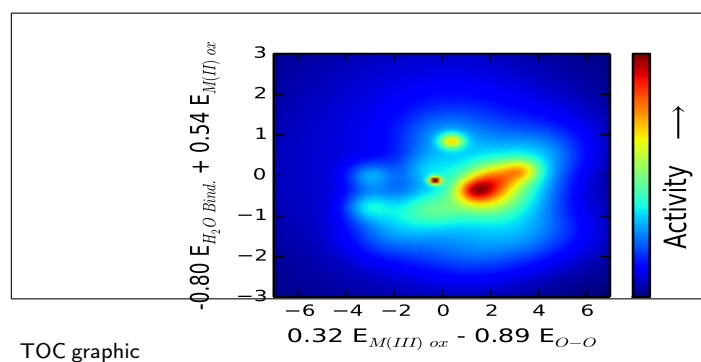
- (55) Jiménez-Hoyos, C. A.; Janesko, B. G.; Scuseria, G. E. Evaluation of Range-Separated Hybrid Density Functionals for the Prediction of Vibrational Frequencies, Infrared Intensities, and Raman Activities. *Phys. Chem. Chem. Phys.* **2008**, *10*, 6621–9.
- (56) Cossi, M.; Rega, N.; Scalmani, G.; Barone, V. Energies, Structures, and Electronic Properties of Molecules in Solution with the C-PCM Solvation Model. *J. Comput. Chem.* **2003**, *24*, 669–681.
- (57) Tomasi, J.; Mennucci, B.; Cammi, R. Quantum Mechanical Continuum Solvation Models. *Chem. Rev.* **2005**, *105*, 2999–3093.
- (58) Cramer, C. J.; Truhlar, D. G. A Universal Approach to Solvent Modeling. *Accounts Chem. Res.* **2008**, *41*, 760–768.
- (59) Klamt, A.; Mennucci, B.; Tomasi, J.; Barone, V.; Curutchet, C.; Orozco, M.; Luque, F. J. On the Performance of Continuum Solvation Methods. A Comment on "Universal Approaches to Solvation Modeling". *Accounts Chem. Res.* **2009**, *42*, 489–492.
- (60) Gilbert, J. A.; Eggleston, D. S.; Murphy, W. R.; Geselowitz, D. A.; Gersten, S. W.; Hodgson, D. J.; Meyer, T. J. Structure and Redox Properties of the Water-Oxidation Catalyst  $[(\text{bpy})_2(\text{OH}_2)\text{RuORu}(\text{OH}_2)(\text{bpy})_2]^{4+}$ . *J. Am. Chem. Soc.* **1985**, *107*, 3855 – 3864.
- (61) Yang, X.; Baik, M.-H. *cis,cis*- $[(\text{bpy})_2\text{RuVO}]_2\text{O}^{4+}$  Catalyzes Water Oxidation Formally Via In Situ Generation of Radicaloid RuIV-O. *J. Am. Chem. Soc.* **2006**, *128*, 7476 – 7485.
- (62) Kobayashi, K.; Ohtsu, H.; Wada, T.; Kato, T.; Tanaka, K. Characterization of a Stable Ruthenium Complex with an Oxyl Radical. *J. Am. Chem. Soc.* **2003**, *125*, 6729 – 6739.

- (63) Bozoglian, F.; Romain, S.; Ertem, M. Z.; Todorova, T. K.; Sens, C.; Mola, J.; Rodriguez, M.; Romero, I.; Benet-Buchholz, J.; Fontrodona, X. et al. The Ru-Hbpp Water Oxidation Catalyst. *J. Am. Chem. Soc.* **2009**, *131*, 15176 – 15187.
- (64) Ghosh, S.; Baik, M.-H. The Mechanism of O-O Bond Formation in Tanaka’s Water Oxidation Catalyst. *Angew. Chem. Intl. Ed.* **2011**, *51*, 1221 – 1224.
- (65) Fujishima, A.; Rao, T. N.; Tryk, D. A. Titanium Dioxide Photocatalysis. *J. Photoch. Photobiol. C* **2000**, *1*, 1–21.
- (66) McCrory, C. C. L.; Jung, S.; Peters, J. C.; Jaramillo, T. F. Benchmarking Heterogeneous Electrocatalysts for the Oxygen Evolution Reaction. *J. Am. Chem. Soc.* **2013**, *135*, 16977–16987.
- (67) Law, J.; Jolliffe, I. T. Principal Component Analysis. *Statistician* **1987**, *36*, 432.
- (68) Kuroki, S.; Nabae, Y.; Chokai, M.; Kakimoto, M. A.; Miyata, S. Oxygen Reduction Activity of Pyrolyzed Polypyrroles Studied by <sup>15</sup>N Solid-State NMR and XPS with Principal Component Analysis. *Carbon* **2012**, *50*, 153–162.
- (69) Wang, H.; Xie, M.; Thia, L.; Fisher, A.; Wang, X. Strategies on the Design of Nitrogen-Doped Graphene. *J. Phys. Chem. Lett* **2014**, *5*, 119–125.
- (70) Fabbri, E.; Haberer, A.; Waltar, K.; Kötzt, R.; Schmidt, T. J.; Kötzt, R.; Schmidt, T. J. Developments and Perspectives of Oxide-Based Catalysts for the Oxygen Evolution Reaction. *Catal. Sci. Tech.* **2014**, *4*, 3800–3821.
- (71) Burke, M. S.; Zou, S.; Enman, L. J.; Kellon, J. E.; Gabor, C. A.; Pledger, E.; Boettcher, S. W. Revised Oxygen Evolution Reaction Activity Trends for First-Row Transition-Metal (Oxy)hydroxides in Alkaline Media. *J. Phys. Chem. Lett.* **2015**, *6*, 3737–3742.
- (72) Halck, N. B.; Petrykin, V.; Krtil, P.; Rossmeisl, J. Beyond the Volcano Limitations in

Electrocatalysis—Oxygen Evolution Reaction. *Phys. Chem. Chem. Phys.* **2014**, *16*, 13682–13688.

- (73) Gorlin, M.; Ferreira de Araujo, J.; Schmeis, H.; Bernsmeier, D.; Dresp, S.; Gliech, M.; Jusys, Z.; Chernev, P.; Kraehnert, R.; Dau, H. et al. Tracking Catalyst Redox States and Reaction Dynamics in Ni-Fe Oxyhydroxide Oxygen Evolution Reaction Electrocatalysts: The Role of Catalyst Support and Electrolyte pH. *J. Am. Chem. Soc.* **2017**, *139*, 2070 – 2082.
- (74) Vaissier, V.; Van Voorhis, T. Adiabatic Approximation in Explicit Solvent Models of RedOx Chemistry. *J. Chem. Theory Comput.* **2016**, *12*, 5111 – 5116.

# Graphical TOC Entry





# Supporting Information for “Computational Design Principles of Two-Center First-Row Transition Metal Oxide Oxygen Evolution Catalysts”

Michael G. Mavros,<sup>†</sup> James J. Shepherd,<sup>†</sup> Takashi Tsuchimochi,<sup>†,‡</sup> Alexandra R. McIsaac,<sup>†,¶</sup> and Troy Van Voorhis\*,<sup>†</sup>

<sup>†</sup>*Department of Chemistry, Massachusetts Institute of Technology, 77 Massachusetts Ave,  
Cambridge, MA 02139 USA*

<sup>‡</sup>*Graduate School of Science, Technology and Innovation, Kobe University, Kobe 657-8501,  
Japan*

E-mail: tvan@mit.edu

Supporting Information for this paper is supplied as a .zip file. The contents is as follows.

- In the folder xyz, .xyz files are given that correspond to the geometries for every molecule
- In file imag-freq-tot.csv, we list the imaginary frequencies for every molecule
- In file mulliken.txt, mulliken charges and spins are listed associated with their corresponding molecule. The columns are as follows:
  - 1) The molecule label
  - 2) Line number of the atom in the xyz file
  - 3) Type of atom

- 4) Mulliken charge
  - 5) Mulliken spin (where available)
  - 6)-9) Nearest neighbor atoms in order of increasing distance
- In file scf\_energies.txt, we list all the scf energies for every molecule

We label the files according to the structures in Fig. 1,(1)-(6) in the main manuscript. The correspondence between the filename conventions laid out in this Supporting Information and the corresponding molecular structures shown in Figure 1 are as follows:

- For homobimetallics:
  - files with oh# correspond to Fig. 1,(1) (# is the number of times we needed to run Q-Chem to obtain convergence)
  - files with o# correspond to Fig. 1,(2)
  - files with long correspond to Fig. 1,(3)
  - files with short correspond to Fig. 1,(4)
  - files with moomohh correspond to Fig. 1,(5)
  - files with oo# correspond to Fig. 1,(6)
  - files with ooh# correspond correspond to the unnumbered structure in Figure 1 that participates exclusively in the acid-base mechanism.
- For homobimetallics:
  - files with moh-moh correspond to Fig. 1,(1) (# is the number of times we needed to run Q-Chem to obtain convergence)
  - files with mo-moh correspond to Fig. 1,(2)
  - files with moh-mo correspond to Fig. 1,(2)
  - files with mo-mo correspond to Fig. 1,(3)
  - files with mo-om correspond to Fig. 1,(4)

- files with moo-mohh correspond to Fig. 1,(5)
- files with mohh-moo correspond to Fig. 1,(5)
- files with moo-moh correspond to Fig. 1,(6)
- files with moh-moo correspond to Fig. 1,(6)
- the proximity of the terminal oxygen group to the metal in the file name dictates connectivity.
  - \* ex: tioh-feoo corresponds to a structure like (6) where -OH is connected to Ti and -OO is connected to Fe.
  - \* ex: tioo-feoh corresponds to a structure like (6) where -OO is connected to Ti and -OH is connected to Fe.